Room temperature synthesis of low-dimensional rubidium copper halide colloidal nanocrystals with near unity photoluminescence quantum yield

Vashishtha, Parth; Hooper, Thomas James Nelson; Fang, Yanan; Deviana, Kathleen; Giovanni, David; Klein, Maciej; Sum, Tze Chien; Mhaisalkar, Subodh Gautam; Mathews, Nripan; White, Tim

2020

Vashishtha, P., Hooper, T. J. N., Fang, Y., Deviana, K., Giovanni, D., Klein, M., ... White, T. (2020). Room temperature synthesis of low-dimensional rubidium copper halide colloidal nanocrystals with near unity photoluminescence quantum yield. Nanoscale. doi:10.1039/D0NR08093D

https://hdl.handle.net/10356/145108

https://doi.org/10.1039/D0NR08093D

Nanoscale

Accepted Manuscript

This article can be cited before page numbers have been issued, to do this please use: P. Vashishtha, T. J. N. Hooper, Y. FANG, K. Deviana, D. Giovanni, M. Klein, T. C. Sum, S. G. Mhaisalkar, N. Mathews and T. White, *Nanoscale*, 2020, DOI: 10.1039/D0NR08093D.

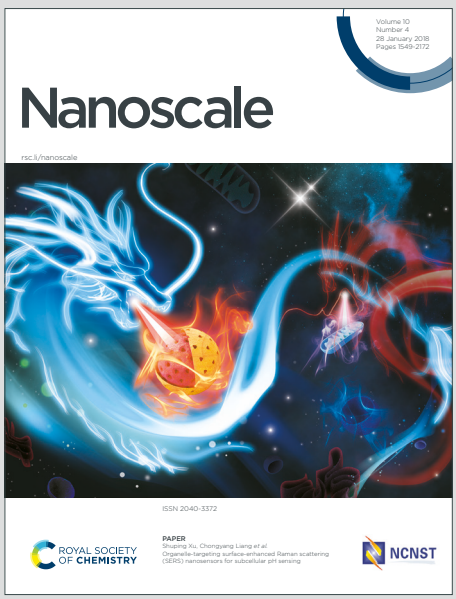

ROYAL SOCIETY OF CHEMISTRY

rsc.li/nanoscale

Room Temperature Synthesis of Low-Dimensional Rubidium Copper Halide Colloidal Nanocrystals with Near Unity Photoluminescence Quantum Yield

Parth Vashishtha[†]*, Thomas J.N. Hooper[‡], Yanan Fang[†], Deviana Kathleen[†], David Giovanni[§], Maciej Klein,[‖§] Tze Chien Sum[§], Subodh G. Mhaisalkar[†‖], Nripan Mathews[†‖]*, and Tim White[†]*

[†]*School of Materials Science and Engineering, Nanyang Technological University (NTU), 50 Nanyang Avenue, Singapore 639798, Republic of Singapore*

[‡]*High Field NMR Facility, School of Physics and Mathematical Sciences, Nanyang Technological University, 21 Nanyang Link, Singapore 637371, Republic of Singapore*

[‖]*Energy Research Institute @NTU (ERI@N), Research Techno Plaza, X-Frontier Block, Level 5, 50 Nanyang Drive, Singapore 637553, Republic of Singapore*

[§]*Division of Physics and Applied Physics, School of Physical and Mathematical Sciences, Nanyang Technological University, 21 Nanyang Link, Singapore 637371, Republic of Singapore*

Abstract

Metal lead halide perovskite nanocrystals have emerged as promising candidates for optoelectronic applications. However, the inclusion of toxic lead is a major concern for the commercial viability of these materials. Herein, we introduce a new family of non-toxic reduced dimension Rb_2CuX_3 (X= Br, Cl) colloidal nanocrystals with one-dimensional crystal structure consisting $[CuX_4]^{3-}$ ribbons isolated by Rb^+ cations. These nanocrystals were synthesised using a room-temperature method under ambient conditions, which makes them cost effective and scalable. Phase purity quantification was confirmed by Rietveld refinement of powder x-ray diffraction and corroborated by ^{87}Rb MAS NMR technique. Both samples also exhibited high thermal stability up to 500°C, which is essential for optoelectronic applications. Rb_2CuBr_3 and Rb_2CuCl_3 displays PL emission peaks at 387 nm and 400 nm with high PLQYs of ~100% and ~49%, respectively. Lastly, the first colloidal synthesis of quantum-confined rubidium copper halide-based nanocrystals opens up a new avenue to exploit their optical properties in lighting technology as well as water sterilisation and air purification.

Introduction

Semiconductor nanocrystals offer several advantages over their bulk counterparts due to quantum confinement which results in improved photoluminescence quantum yield (PLQY), narrow emission line-width, surface functionality, and size tunable emission wavelength.[1-4] In the last decade, significant efforts have been made to not only improve the synthesis of nanocrystals but also to find novel nanocrystals with desirable optical properties.[5-10] Among them, metal halide perovskite nanocrystals, such as $CsPbX_3$, $MAPbX_3$, $FAPbX_3$ (FA= formamidinium, MA= methylammonium, X= Cl, Br, I), have emerged as a new class of most promising candidates for optoelectronic applications.[9, 11-15] In particular, due to the pure inorganic structure of $CsPbX_3$ nanocrystals, high thermal stability can be achieved alongside their characteristic advantages of near unity PLQY and low processing cost.[12, 16-18] Therefore, research into other possible inorganic perovskite structures, such as Cs_4PbBr_6 and $Rb_yCs_{1-y}PbBr_3$, has intensified.[19, 20] However, the commercial viability of these materials are limited due to the toxicity of lead, resulting in the pursuit of lead-free nanocrystals. The most obvious alternative was stannous based perovskite nanocrystals ($CsSnX_3$), due to the favoured transformation of Sn^{2+} to Sn^{4+}, these materials were found to be too unstable.[21] Similarly, many other nanocrystals such as $Cs_3Sb_2X_9$,[22] $Cs_3Bi_2I_9$,[23] $Cs_2AgInCl_6$,[24] $Cs_2AgSbCl_6$,[25] and $Cs_2AgBiCl_6$[25] remain ambiguous for lighting applications.

Reduced-dimensional $Cs_3Cu_2I_5$ lead-free metal halide crystal structures consists isolated octahedra which causes high exciton binding energies (~490 eV) as a result of exciton confinement within each octahedra.[26] Thus, higher exciton binding energies pave the way for high PLQYs in this class of materials.[26] Recently, nanocrystals of Cs_3CuCl_5 (PL= 521 nm), Cs_3CuBr_5 (PL= 458 nm), Cs_3CuI_5 (PL= 453 nm), and $CsCu_2I_3$ (PL= 570 nm) with high PLQY and room temperature phase stability were obtained in our previous reports.[27, 28] These materials demonstrated pure white emission as a result of colour tunable emission wavelengths and reduced halide segregation- an effect which is unavoidable in lead-based perovskite materials.[27] After the development of cesium copper halide nanocrystals,

research towards developing similar copper based metal halide nanocrystals have garnered tremendous attention.[29] Another alternate could be rubidium copper halide (Rb_2CuX_3), which exhibits large band gaps and emission in the UVA spectral region (380–400 nm).[30] Rb_2CuX_3 has one dimensional crystal structures demonstrating $[CuX_4]3^-$ ribbons isolated by Rb^+ cations. Yang *et al.* were the first to report the bulk crystals of Rb_2CuBr_3, synthesised using an acidic medium at high temperature for application in X-ray scintillators.[31] Later, Creason *et al.* used a solid state method to synthesize bulk pellets of Rb_2CuX_3 (X = Cl, Br) for up-conversion.[30] Both samples displayed high PL quantum yield (>60%) with PL peak position at 386 nm and 400 nm for Rb_2CuBr_3 and Rb_2CuCl_3, respectively.[30] These materials also exhibited a large stoke shift of 85 nm for Rb_2CuBr_3 and 93 nm for Rb_2CuCl_3, indicating potential applications in solid-state or phosphor-based lighting.[7] However, the synthesis of Rb_2CuX_3 in the form of colloidal nanocrystals has not been developed, despite the fact that colloidal nanocrystals offer several advantages over bulk crystals in term of easier solution processability, and superior optical structural properties, as described earlier.[28, 31] To date, there is no report of solution processed room temperature syntheses of Rb_2CuX_3 colloidal nanocrystals.

This work describes the first synthesis of colloidal Rb_2CuX_3 (X= Cl, Br) nanocrystals using a room-temperature ligand assisted re-precipitation (LARP) method. A detailed quantitative structural analysis was performed via powder x-ray diffraction followed by Rietveld refinement. Additionally, solid-state NMR was utilized to investigate the local structure and surface properties, while indirectly validating that Cu is formed in the Cu(I) oxidation state in the bulk of each nanocrystal. Thermogravimetric analysis (TGA) measurements were performed to probe the thermal stability of these materials for optoelectronic applications. Optical properties of the colloidal nanocrystal solutions was analysed using static-state absorption and photoluminescence spectroscopy followed by analysis of PLQY.

Results and Discussion

Colloidal nanocrystals of Rb_2CuX_3 were synthesized via a room temperature ligand assisted re-precipitation (LARP) method. In this method, the halide precursor salts of RbX (X= Cl, Br), and CuX

were firstly dissolved in dimethyl sulfoxide solvent. After that, the precursor solution was added dropwise to a solution of toluene and oleic acid ligands, which resulted in the formation of the nanocrystals. After 5 minutes, the reaction was stopped, the nanocrystals were purified and finally dissolved in iso-propanol (IPA) to prepare a colloidal solution (See Experimental section for further details).

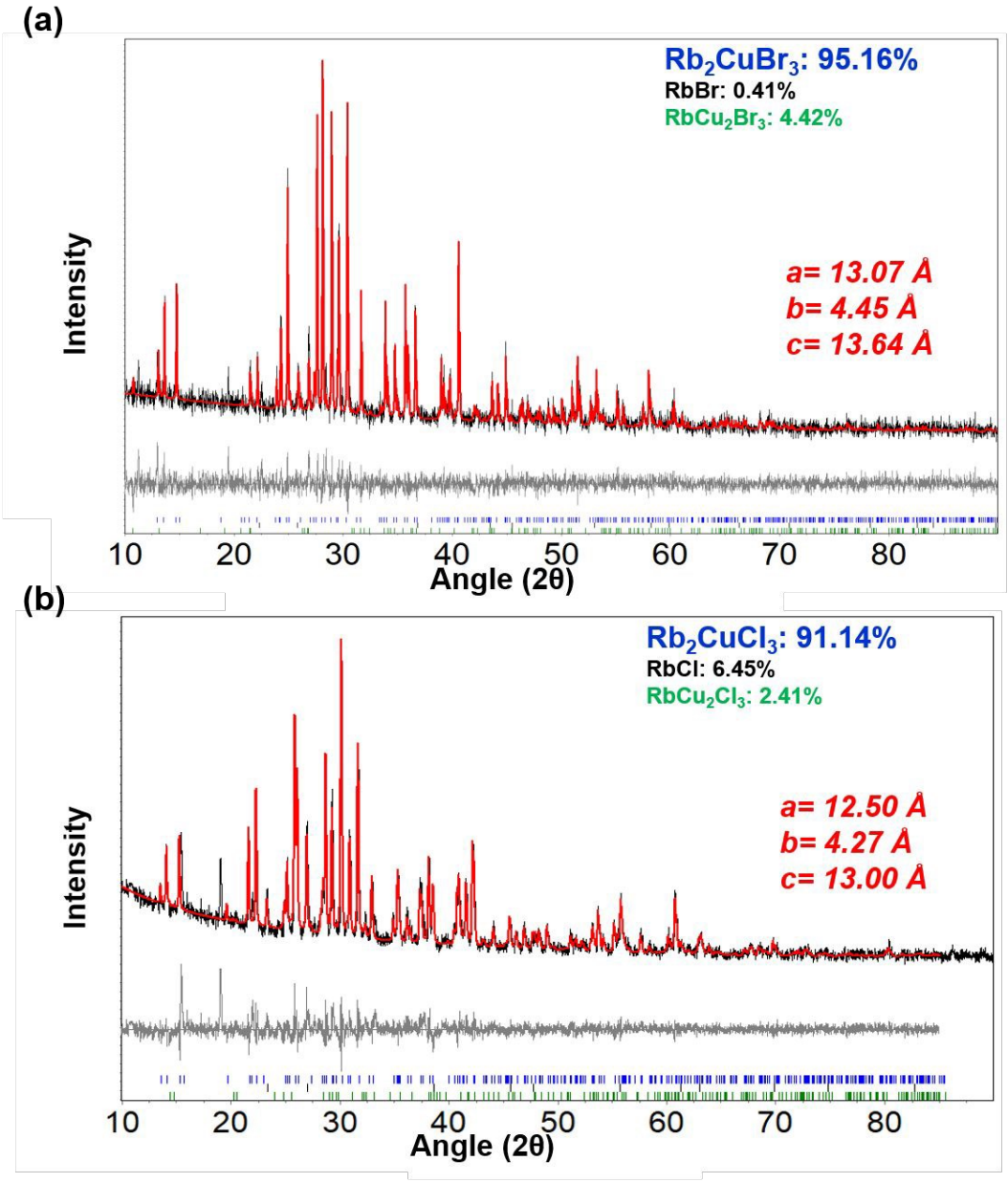

Figure 1. *Powder XRD Pattern (black lines) of (a) Rb_2CuBr_3 and (b) Rb_2CuCl_3 nanocrystals with Rietveld refinement fits (red lines) using TOPAS and residual maps of both graphs (gray lines).*

Nanocrystals were characterized using powder XRD to analyse the crystallographic properties. Figures 1(a,b) depict the diffraction pattern of Rb_2CuBr_3 and Rb_2CuCl_3 nanocrystals. Rietveld refinement using

TOPAS confirmed the orthorhombic crystal structure of Rb_2CuBr_3 (Pnma) and Rb_2CuCl_3 (Pnma) with lattice parameters of a= 13.0786 Å, b= 4.4518 Å, c= 13.6465 Å and a= 12.5084 Å, b= 4.2741 Å, c= 13.0085 Å, respectively. The cell parameters are listed in Table S1 and S2. Expected peak broadening due to nanocrystallinity was not completely observed as the samples were prepared by vacuum drying nanocrystal powders to clearly observe all of the reflection for phase identification, which is also consistent with XRD patterns of other reduced dimensional copper halide colloidal nanocrystals.[28, 32-35] Additionally, Rietveld refinement revealed some phase impurity of RbBr (0.4%), and $RbCu_2Br_3$ (4.4%) in the Rb_2CuBr_3 sample and RbCl (6.4%), and $RbCu_2Cl_3$ (2.4%) in the Rb_2CuCl_3 sample. However, the total amount of impurity is less than 9% in both samples. A diagram identifying each peak individually is presented in Figure S1. A phase degradation study over 6 days under ambient conditions using XRD on these nanocrystals explained that the Cu^+ slowly oxidizes to Cu^{2+}. It was found that within 6 days 77% of the Rb_2CuCl_3 had slowly degraded to $RbCuCl_3$ (42%) and RbCl (35%); in contrast, only 17% of Rb_2CuBr_3 had degraded to $CuBr_2$ (13%) and RbBr (4%) over 6 days (Figure S2 and Table 1). The faster degradation of Rb_2CuCl_3, in comparison to Rb_2CuBr_3, can be attributed to the higher hygroscopicity of RbCl than that of RbBr. Therefore, the degradation of these materials could be due to the absorption of moisture, which leads to the oxidation of Cu^+ structures to Cu^{2+} structures and also the decomposition to RbBr/RbCl.[30] Moreover, X-ray Photoelectron Spectroscopy (XPS) study of Rb_2CuBr_3 reveals that copper core-level spectrum consists a 2p doublet for copper core-level spectrum has binding energies of 931.7 eV (2p3/2) and 951.5 eV (2p1/2) with a separation of 19.7 eV, which is consistent with Cu^+ (Figure S4a).[36, 37] Similarly, Cu 2p XPS spectrum for Rb_2CuCl_3 shows 2p doublet with the binding energies of 934.6 eV (2p3/2) and 954.3 eV (2p1/2) with a separation of 19.7 eV, corresponding to Cu^+.[31, 36] However, Cu2p XPS spectrum of Rb_2CuCl_3 also shows strong cu^{2+} satelite peak, which indiactes the surface oxidation in Rb_2CuCl_3 nanocrystals.[37] A noticable color change of the nanocrystal powders from white to green/yellow was observed after a few hours under ambient conditions. Despite being susceptible to degradation in powder form, the colloidal solution of these nanocrystals was found to be stable over a week (white colored transparent liquid). Figure 2 shows the crystal structure of both samples. In the typical crystal structure, the Cu atom is surrounded by four bromine/chlorine atoms as a $[CuX_4]^{3-}$ tetrahedron (blue or yellow colour). As depcited in the bottom panel of Figure 2, these tetrahedrons form corner-sharing one dimensional chain along the <010> plane separated by Rb^+ cations. The synthesis of $Rb_2Cu(Br/Cl)_3$ was also attempted, however the yield was small with many side products formed (Figure S1c), suggesting further research is required to optimize the mixed-halide phase.

View Article Online
DOI: 10.1039/D0NR08093D

Table 1. Phase degradation of Rb_2CuBr_3 and Rb_2CuCl_3 nanocrystal powder under ambient conditions

Rb_2CuBr_3 nanocrystals				
Time (days)	Rb_2CuBr_3 (wt%)	$RbCu_2Br_3$ (wt%)	RbBr (wt%)	$CuBr_2$ (wt%)
0 days	95.16	4.42	0.41	-
3 days	87.17	-	3.46	9.37
6 days	83.13	-	4.01	12.87
Rb_2CuCl_3 nanocrystals				
Time (days)	Rb_2CuCl_3 (wt%)	$RbCu_2Cl_3$ (wt%)	RbCl (wt%)	$RbCuCl_3$ (wt%)
0 days	91.14	2.41	6.45	-
3 days	88.78	-	5.31	5.91
6 days	23.43	-	34.40	42.17

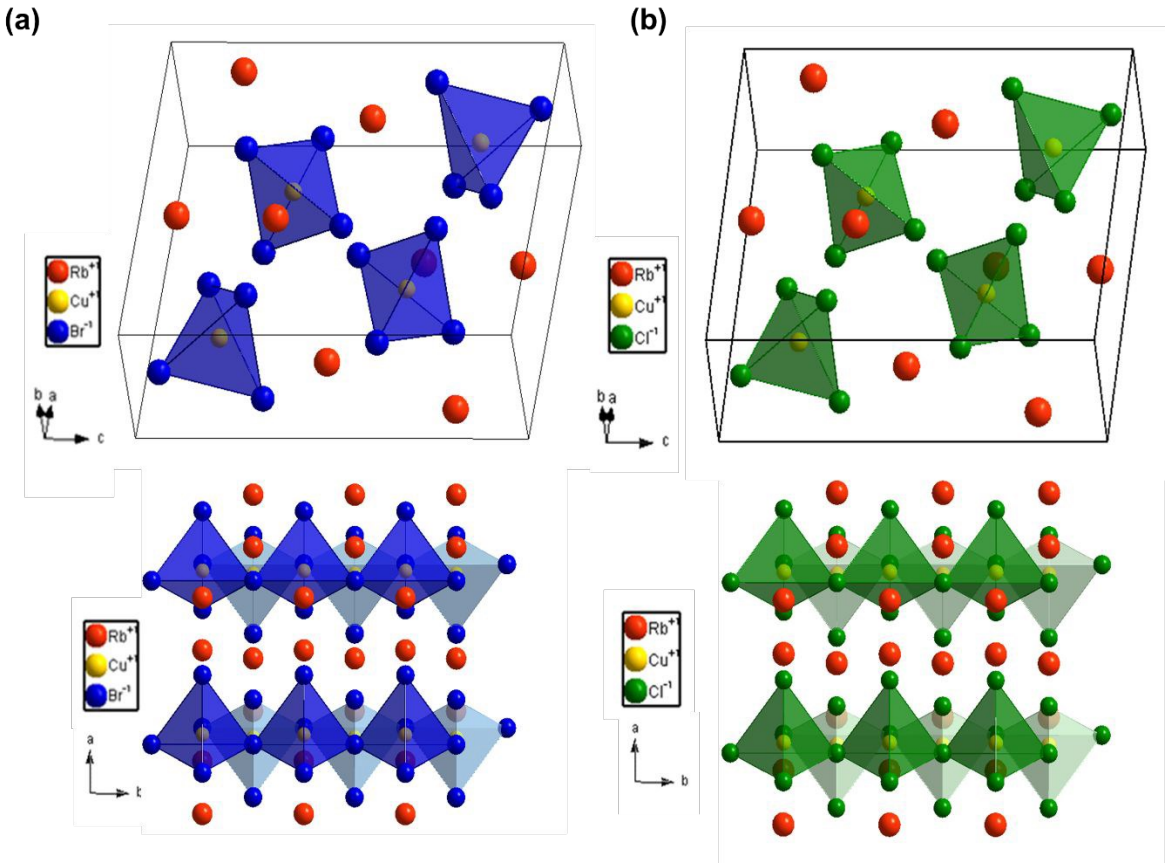

***Figure* 2**. *Crystal structures of (a) Rb_2CuBr_3 and (b) Rb_2CuCl_3 nanocrystals with optimized lattice parameters. As clearly evident in the bottom panel, both structures exhibit $[CuX_4]^{3-}$ chains isolated by Rb^+ cations forming a one dimensional crystal structure.*

The nanocrystals were examined using transmission electron microscopy (TEM) to analyse the morphology and size. Figure 3 depicts the TEM micrographs of $Rb_2Cu_2Br_3$ and $Rb_2Cu_2Cl_3$ nanocrystals. Both samples showed nanoplate-like faceted morphology with an average size of ~7.7 nm for Rb_2CuBr_3 and ~7.5 nm for Rb_2CuCl_3 (Figure 3 and S3). An average shifted histogram (Figure 3c and f) and a standard historgam (Figure S3c and f) are plotted for the illustration of particle size distrubution. High-resolution TEM and fast Fourier transform (FFT) (Figure 3b and e) gives lattice spacings of 2.2 Å and 2.1 Å for Rb_2CuBr_3 and Rb_2CuCl_3 nanocrystals, respectively. Matching of FFT with corresponding diffraction patterns plane of both samples reverify the formation of Rb_2CuX_3 crystal structure. Elemental analysis via energy dispersive x-ray spectroscopy (EDXS) revealed atomic ratios of 1.97:1.00:3.01 for Rb_2CuBr_3 and 1.96:1.00:2.95 Rb_2CuCl_3 nanocrystals (Figure S3g, S3h and Table S3).

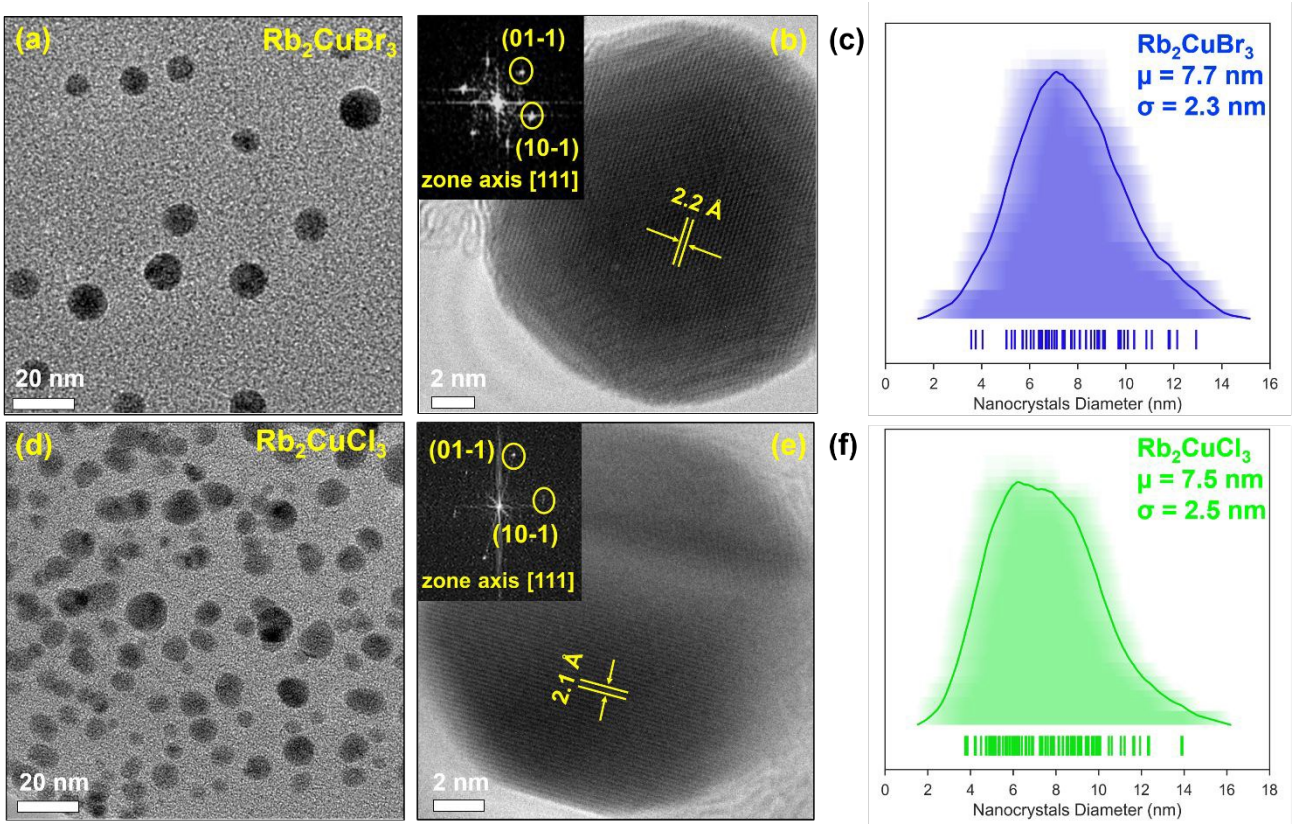

Figure 3. *Transmission electron micrographs of (a) Rb_2CuBr_3 and (d) Rb_2CuCl_3 nanocrystals, including high resolution TEM image of both samples depicting the lattice place of (b) Rb_2CuBr_3 and (e) Rb_2CuCl_3 nanocrystals with an inset of fast Fourier transform (FFT) images showing the crystallinity and planes of both nanocrystals sample in (b) for Rb_2CuBr_3 and (e) Rb_2CuCl_3. Particle*

size of both sample measured as mean diameter was estimated via an average shifted histogram of (c) Rb_2CuBr_3 and (f) Rb_2CuCl_3 nanocrystals.

Solid state NMR was also utilized to help further characterise the nanocrystal powders. ^{87}Rb MAS NMR of both nanocrystal samples is shown in Figure 4, alongside the spectra of the halide precursor salts RbBr and RbCl. The Rb_2CuBr_3 NCs spectrum presents with a dominant resonance at 124 ppm assigned to the Rb_2CuBr_3 phase. A smaller resonance at 159 ppm is identical to the resonance given by the pure RbBr powder, and hence can be assigned as the RbBr impurity, detected by XRD. The ^{87}Rb MAS NMR of the Rb_2CuCl_3 nanocrystal sample presents a singular narrow resonance at 104 ppm. The Rb_2CuCl_3 resonance is shifted to lower frequency than the corresponding Rb_2CuBr_3 resonance which is analagous to the shift difference between RbBr and RbCl. The narrowness of the Rb2CuX3 resonances demonstrates the relatively symmetrical environment about the Rb site within the channels created by the 1D $[CuX^4]^{3-}$ chains, as no quadrupolar effect is observed. The impurities of RbCl and $RbCu_2X_3$ observed in the XRD of the nanocrystal powders are presumed to have a small enough concentration that they cannot be seen above the noise in the ^{87}Rb spectra. In addition, the lack of any observed effect from paramagentic centres on the ^{87}Rb NMR, as demonstrated by the relatively unchanged ^{87}Rb spin-lattice relaxation times (Table S4), indirectly confirms that $RbCu(II)X_3$ phases are not present in the fresh powder samples. The ^{1}H MAS NMR of both samples (Figure S4b) also reveals that the oleic acid ligands responsible for the nanocrystal formation are still present in the nanocrystal powders.

Collectively, XRD, TEM, EDXS, and NMR have confirmed the formation of Rb_2CuX_3 nanocrystals with an orthorhombic crystal structure and faceted nanocrystal morphology, with particle sizes less than 10 nm.

View Article Online
DOI: 10.1039/D0NR08093D

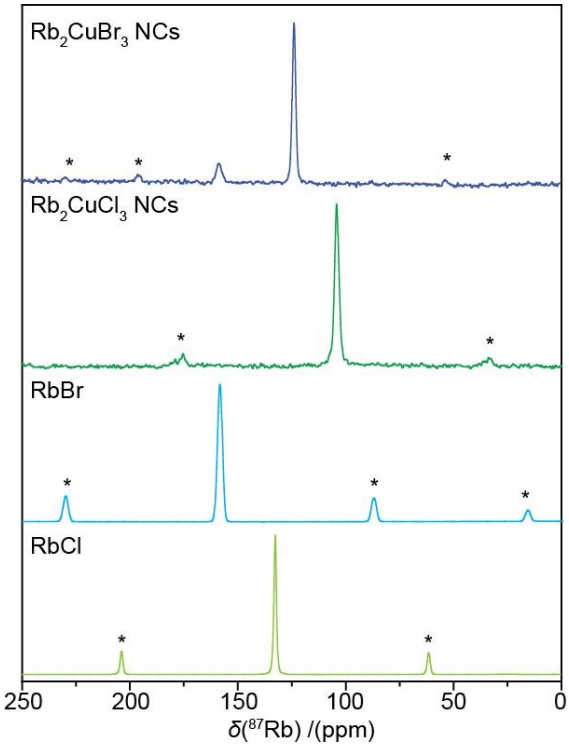

Figure 4. *The ^{87}Rb MAS NMR of Rb_2CuBr_3 (blue line) and Rb_2CuCl_3 (green line) nanocrystal powders in comparison to pure powders of RbBr (cyan line) and RbCl (light-green line) (spinning sidebands are marked by asterisks).*

Rb_2CuBr_3 and Rb_2CuCl_3 Colloidal solutions exhibit strong absorption at 276 nm and 265 nm respectively, which is ~20 nm blue shifted compared to the reported absorption profile of the bulk materials and single crystals (Figure S5a).[30, 31] Rb_2CuBr_3 and Rb_2CuCl_3 exhibits an excitation peak at 292 nm and 285 nm (Figure 5a and b), confirming the excitation is due to the excitonic absorption. As depicted in Figure 5a and b, Rb_2CuBr_3 shows an emission peak at 387 nm with fwhm of 50 nm, whereas Rb_2CuCl_3 shows an emission peak at 400 nm with a fwhm of 52 nm. These nanocrystals show extremely bright violet colour under 300 nm UV excitation (Figure 5c) with PLQY of ~100% and 49% for Rb_2CuBr_3 and Rb_2CuCl_3, respectively. The lower PLQY of Rb_2CuCl_3 sample can be attributed to structural defects of metal chloride based materials; which has also been observed in chlorine-based perovskite.[38, 39] In order to confirm there is no emission from mixed phases, excitation dependent PL spectra was measured (Figure S5b and c). However no peak shift in emission spectra was observed, confirming the emission source is the main product Rb_2CuX_3 in both samples. A large stoke shift in

both nanocrystals has also been observed in previous studies of bulk materials, which suggests that the emission is not due to band to band emission.[30] The excitation and emission spectral features are quite similar, which confirms that the PL originates from the relaxation of the same excited state. Time-resolved PL measurements were conducted to measure the carrier lifetime of these nanocrystals. As depicted in Figure 5c, Rb_2CuBr_3 nanocrystals exhibited a long carrier lifetime of 46.7 μs, whereas Rb_2CuCl_3 exhibits a carrier lifetime of 9.9 μs, which is consistent with their bulk counterparts.[30, 31] Figure S7a shows the linear dependency of PL intensity with excitation power, suggesting the PL does not arise from a permanent defect.[34, 40] Whereas, the long carrier lifetime is due to self-trapped exciton emission mechanism in these materials.[30, 31] It should be noted that other copper halide systems such as $Cs_3Cu_2X_5$ and $CsCu_2X_3$ also display similar microsecond carrier lifetimes.[28] Moreover, It was found that these materials have very high Huang-Rhys factors, which make them more susceptible for the formation of self-trapped excitons (STEs).[31] Under light illumination, copper halide based materials are found to undergo structural reorganization such that the Cu(I)-$3d^{10}$ forms Cu(II)-$3d^9$ and induces strong Jahn-Teller distortion.[26-28] Overall, the energy difference between Cu(II) and Cu(I) causes the large stokes shift. Similar large stoke shift and STE emission mechanism were observed in other low-dimensional materials such as $Cs_2Ag_xNa_{1-x}InCl_6$:Bi, $Cs_3Cu_2X_5$, $(C_4N_2H_{14}X)_4SnX_6$, $C_4N_2H_{14}PbBr_4$, and $CsCu_2I_3$.[26-28, 41-43] On another note, due to the large stoke shift, there is nearly no overlap between the excitation and emission spectra in these nanocrystals, making them ideal candidates for phosphor-based solid-state lighting application.[44]

Colloidal stability of these nanocrystals was found to be reasonably stable up to 2 days in ambient conditions. Moreover, the colloidal solutions of the Rb_2CuBr_3 and Rb_2CuCl_3 nanocrystals displayed up to 13% and 50% reduction in photoluminescence quantum yield, respectively, after storage under ambient conditions. (Figure S6). The faster PL degradation in Rb_2CuCl_3 can be attributed to the surface oxidation due to high hygroscopicity of Rb_2CuCl_3 sample as observed by XPS spectra (Figure S4a). These nanocrystals were successfully incorporated in PDMS polymer matrix (Figure S7b), which

demonstrate their compatibility to form white display devices with YAG yellow phosphor. Materials with potential application in semiconductor devices must also exhibit high thermal stability. The same nanocrystals embedded in a PDMS matrix were utilized for temperature dependent in-situ PL measurements. Albeit, the temperature-dependent PL measurement shows the 50% intensity degradation at 100°C (Figure S7b), which could be due to the enhanced non-radiative recombination induced by thermal energy.[45] Thermal decomposition stability of the Rb_2CuX_3 nanocrystal powders using TGA measurements showed some promising results (Figure 5d). As depicted in Figure 5d, weight loss up to 250°C can be attributed to the loss of organic ligands from the surface of the nanocrystals. The TGA curve also reveals that the Rb_2CuBr_3 exhibits remarkably high thermal stability up to 750°C, 200°C higher than the Rb2CuCl3 nanocrystals. Regardless, both samples show high thermal stability up to 550°C, which is desirable for optoelectronic applications.

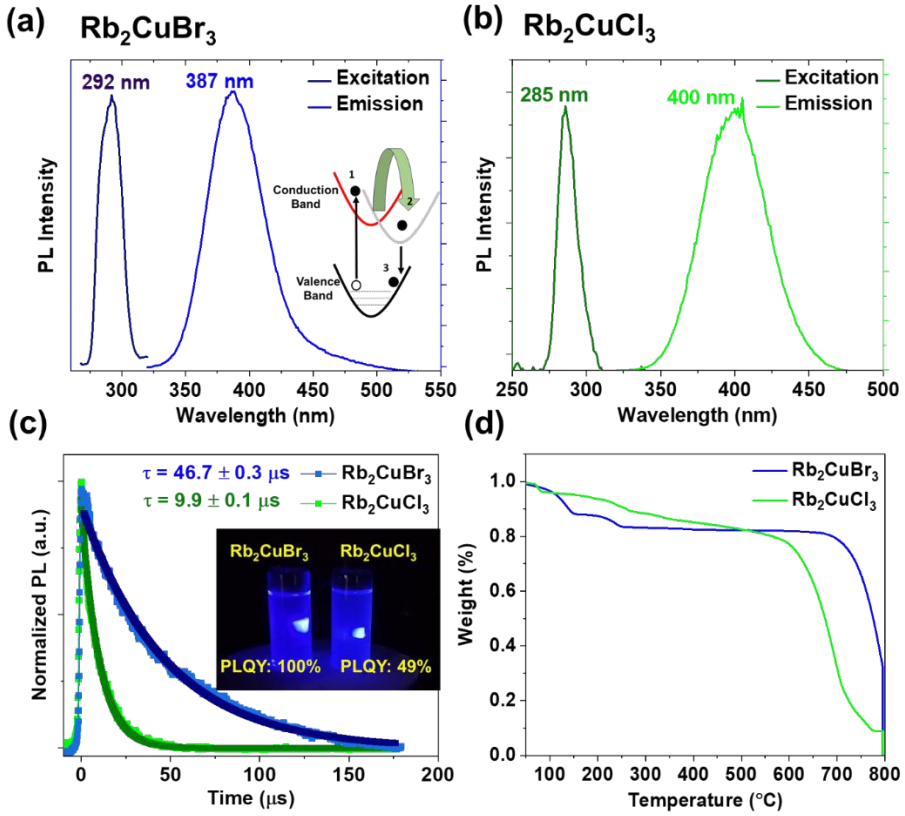

Figure 5. *PL excitation and emission spectra of (a) Rb_2CuBr_3 with an inset schematic presenting the self-trapped exciton emission mechanism and (b) Rb_2CuCl_3 nanocrystals, (c) a photograph of the*

colloidal solution of both nanocrystals in iso-propyl alcohol under 300 nm UV lamp, and (d) thermogravimetric analysis of both samples featuring the high thermal decomposition stability.

Conclusion

This work describes the first synthesis of colloidal Rb_2CuBr_3 and Rb_2CuCl_3 nanocrystals using a room-temperature scalable LARP method. Rietveld refinement of the powder XRD diffraction pattern confirms the Pnma orthorhombic phase purity and provides detailed crystallographic information in these nanocrystals. Solid-state NMR was utilized to analyse the local environment and to confirm the presence of oleic acid ligands. Both of these nanocrystals show remarkably high photoluminescence quantum yield up to 78% in the violet spectral region with a large difference between excitation and emission spectra, making them suitable for phosphor based lighting applications. More importantly, these nanocrystals exhibit high thermal stability up to 550°C. Lastly, despite the need of device optimization, we are confident that the application of these nanocrystals can be extended to stable LEDs.

Acknowledgements

P.V. acknowledges a Presidential Postdoctoral Fellowship from Nanyang Technological University (NTU), Singapore via grant 04INS000581C150OOE01. M.K., N.M., S.G.M., and T.W. acknowledge financial support from the Singapore National Research Foundation, Prime Minister's Office, through the Competitive Research Program (CRP Award No. NRF-CRP14-2014-03). T.C.S and D.G. acknowledge the financial support from the NRF Investigatorship (NRF-NRFI-2018-04) and the Ministry of Education under its AcRF Tier 1 grant (RG91/19) and Tier 2 grant MOE2019-T2-1-006. The authors would like to acknowledge the Facility for Analysis, Characterization, Testing and Simulation (FACTS) at NTU, Singapore, for use of their electron microscopy and X-ray diffraction facilities. We would also like to acknowledge the NTU Centre of High Field NMR Spectroscopy and

View Article Online
DOI: 10.1039/D0NR08093D

Imaging for the use of their NMR facilities. We thank Mr. Sai S. H. Dintakurti and Dr. Ankit, NTU, Singapore.

References:

1. P. O. Anikeeva, J. E. Halpert, M. G. Bawendi and V. Bulovic, *Nano letters*, 2009, **9**, 2532-2536.
2. P. O. Anikeeva, J. E. Halpert, M. G. Bawendi and V. Bulović, *Nano Letters*, 2007, **7**, 2196-2200.
3. Q. Sun, Y. A. Wang, L. S. Li, D. Wang, T. Zhu, J. Xu, C. Yang and Y. Li, *Nature photonics*, 2007, **1**, 717-722.
4. P. Ramasamy, N. Kim, Y.-S. Kang, O. Ramirez and J.-S. Lee, *Chemistry of Materials*, 2017, **29**, 6893-6899.
5. D. W. Ayele, H. M. Chen, W. N. Su, C. J. Pan, L. Y. Chen, H. L. Chou, J. H. Cheng, B. J. Hwang and J. F. Lee, *Chemistry–A European Journal*, 2011, **17**, 5737-5744.
6. D. V. Talapin, I. Mekis, S. Götzinger, A. Kornowski, O. Benson and H. Weller, *The Journal of Physical Chemistry B*, 2004, **108**, 18826-18831.
7. J. Zhou, M. Zhu, R. Meng, H. Qin and X. Peng, *Journal of the American Chemical Society*, 2017, **139**, 16556-16567.
8. L. Protesescu, S. Yakunin, M. I. Bodnarchuk, F. Krieg, R. Caputo, C. H. Hendon, R. X. Yang, A. Walsh and M. V. Kovalenko, *Nano letters*, 2015, **15**, 3692-3696.
9. J. Butkus, P. Vashishtha, K. Chen, J. K. Gallaher, S. K. Prasad, D. Z. Metin, G. Laufersky, N. Gaston, J. E. Halpert and J. M. Hodgkiss, *Chemistry of Materials*, 2017, **29**, 3644-3652.
10. D. Chen, S. Zhou, F. Tian, H. Ke, N. Jiang, S. Wang, Y. Peng and Y. Liu, *Advanced Optical Materials*, 2019, **7**, 1901082.
11. P. Vashishtha, S. A. Veldhuis, S. S. Dintakurti, N. L. Kelly, B. E. Griffith, A. A. Brown, M. S. Ansari, A. Bruno, N. Mathews and Y. Fang, *Journal of Materials Chemistry C*, 2020, **8**, 11805-11821.
12. A. A. M. Brown, T. J. N. Hooper, S. A. Veldhuis, X. Y. Chin, A. Bruno, P. Vashishtha, J. N. Tey, L. Jiang, B. Damodaran and S. H. Pu, *Nanoscale*, 2019.
13. X. Y. Chin, A. Perumal, A. Bruno, N. Yantara, S. A. Veldhuis, L. Martínez-Sarti, B. Chandran, V. Chirvony, A. S.-Z. Lo and J. So, *Energy & Environmental Science*, 2018, **11**, 1770-1778.
14. Y. Ma, P. Vashishtha, K. Chen, E. L. Peach, D. Ohayon, J. M. Hodgkiss and J. E. Halpert, *ChemSusChem*, 2017, **10**, 2677-2684.
15. P. Vashishtha, S. Bishnoi, C. H. A. Li, M. Jagadeeswararao, T. J. N. Hooper, N. Lohia, S. B. Shivarudraiah, M. S. Ansari, S. N. Sharma and J. E. Halpert, *ACS Applied Electronic Materials*, 2020, DOI: 10.1021/acsaelm.0c00825.
16. M. Imran, P. Ijaz, L. Goldoni, D. Maggioni, U. Petralanda, M. Prato, G. Almeida, I. Infante and L. Manna, *ACS Energy Letters*, 2019, **4**, 819-824.
17. R. R. Tamming, J. Butkus, M. B. Price, P. Vashishtha, S. K. Prasad, J. E. Halpert, K. Chen and J. M. Hodgkiss, *ACS Photonics*, 2019, **6**, 345-350.
18. D. Chen and X. Chen, *Journal of Materials Chemistry C*, 2019, **7**, 1413-1446.
19. J. W. Xiao, Y. Liang, S. Zhang, Y. Zhao, Y. Li and Q. Chen, *Chemistry–A European Journal*, 2019, **25**, 2597-2603.
20. X. Du, G. Wu, J. Cheng, H. Dang, K. Ma, Y.-W. Zhang, P.-F. Tan and S. Chen, *RSC advances*, 2017, **7**, 10391-10396.
21. T. C. Jellicoe, J. M. Richter, H. F. Glass, M. Tabachnyk, R. Brady, S. n. E. Dutton, A. Rao, R. H. Friend, D. Credgington and N. C. Greenham, *Journal of the American Chemical Society*, 2016, **138**, 2941-2944.
22. J. Zhang, Y. Yang, H. Deng, U. Farooq, X. Yang, J. Khan, J. Tang and H. Song, *Acs Nano*, 2017, **11**, 9294-9302.
23. G. M. Paternò, N. Mishra, A. J. Barker, Z. Dang, G. Lanzani, L. Manna and A. Petrozza, *Advanced Functional Materials*, 2019, **29**, 1805299.
24. F. Locardi, M. Cirignano, D. Baranov, Z. Dang, M. Prato, F. Drago, M. Ferretti, V. Pinchetti, M. Fanciulli and S. Brovelli, *Journal of the American Chemical Society*, 2018, **140**, 12989-12995.
25. A. NAG and A. S. KSHIRSAGAR, 2019.

26. T. Jun, K. Sim, S. Iimura, M. Sasase, H. Kamioka, J. Kim and H. Hosono, *Advanced Materials*, 2018, **30**, 1804547.
27. P. Vashishtha, G. V. Nutan, B. E. Griffith, Y. Fang, D. Giovanni, M. Jagadeeswararao, T. C. Sum, N. Mathews, S. G. Mhaisalkar and J. V. Hanna, *Chemistry of Materials*, 2019, **31**, 9003-9011.
28. Y. Li, P. Vashishtha, Z. Zhou, Z. Li, S. B. Shivarudraiah, C. Ma, J. Liu, K. S. Wong, H. Su and J. E. Halpert, *Chemistry of Materials*, 2020.
29. Z. Guo, J. Li, R. Pan, J. Cheng, R. Chen and T. He, *Nanoscale*, 2020, **12**, 15560-15576.
30. T. D. Creason, A. Yangui, R. Roccanova, A. Strom, M. H. Du and B. Saparov, *Advanced Optical Materials*, 2020, **8**, 1901338.
31. B. Yang, L. Yin, G. Niu, J. H. Yuan, K. H. Xue, Z. Tan, X. S. Miao, M. Niu, X. Du and H. Song, *Advanced Materials*, 2019, **31**, 1904711.
32. L. Wang, Z. Shi, Z. Ma, D. Yang, F. Zhang, X. Ji, M. Wang, X. Chen, G. Na and S. Chen, *Nano Letters*, 2020, **20**, 3568-3576.
33. P. Vashishtha, G. V. Nutan, B. E. Griffith, Y. Fang, D. Giovanni, M. Jagadeeswararao, T. C. Sum, N. Mathews, S. G. Mhaisalkar and J. V. Hanna, *Chemistry of Materials*, 2019.
34. P. Cheng, L. Sun, L. Feng, S. Yang, Y. Yang, D. Zheng, Y. Zhao, Y. Sang, R. Zhang and D. Wei, *Angewandte Chemie*, 2019, **131**, 16233-16237.
35. E. P. Booker, J. T. Griffiths, L. Eyre, C. Ducati, N. C. Greenham and N. J. Davis, *The Journal of Physical Chemistry C*, 2019, **123**, 16951-16956.
36. H. Su, Y. Xie, S. Wan, B. Li and Y. Qian, *Solid State Ionics*, 1999, **123**, 319-324.
37. X. Jiang, J. Qiao, I. M. Lo, L. Wang, X. Guan, Z. Lu, G. Zhou and C. Xu, *Journal of hazardous materials*, 2015, **283**, 880-887.
38. R. K. Behera, S. Das Adhikari, S. K. Dutta, A. Dutta and N. Pradhan, *The journal of physical chemistry letters*, 2018, **9**, 6884-6891.
39. J. Kim, C.-H. Chung and K.-H. Hong, *Physical Chemistry Chemical Physics*, 2016, **18**, 27143-27147.
40. E. R. Dohner, A. Jaffe, L. R. Bradshaw and H. I. Karunadasa, *Journal of the American Chemical Society*, 2014, **136**, 13154-13157.
41. J. Luo, X. Wang, S. Li, J. Liu, Y. Guo, G. Niu, L. Yao, Y. Fu, L. Gao and Q. Dong, *Nature*, 2018, **563**, 541-545.
42. Z. Yuan, C. Zhou, Y. Tian, Y. Shu, J. Messier, J. C. Wang, L. J. Van De Burgt, K. Kountouriotis, Y. Xin and E. Holt, *Nature communications*, 2017, **8**, 14051.
43. C. Zhou, H. Lin, Y. Tian, Z. Yuan, R. Clark, B. Chen, L. J. van de Burgt, J. C. Wang, Y. Zhou and K. Hanson, *Chemical science*, 2018, **9**, 586-593.
44. M. Ghate, H. Dahule, N. T. Kalyani and S. Dhoble, *Optik*, 2017, **149**, 198-205.
45. J. P. Freedman, J. H. Leach, E. A. Preble, Z. Sitar, R. F. Davis and J. A. Malen, *Scientific reports*, 2013, **3**, 1-6.

View Article Online
DOI: 10.1039/D0NR08093D

TOC